JOURNAL OF GEOPHYSICAL RESEARCH, VOL. 101, NO. A1, PAGES 479–493, JANUARY 1, 1996

Generation of dynamic pressure pulses downstream of the bow shock by variations in the interplanetary magnetic field orientation

Y. Lin, L. C. Lee, [1] and M. Yan [2]

Physics Department, Auburn University, Auburn, Alabama

Abstract. One-dimensional resistive MHD and hybrid simulations are carried out to study the manner by which variations of the interplanetary magnetic field (IMF) direction generate dynamic pressure pulses in the magnetosheath. The reaction of the magnetosheath to the temporal IMF variation is modeled as the interaction between the bow shock (BS) and an interplanetary rotational discontinuity (RD), an Alfven wave pulse (AW), or an Alfven wave train. The resistive MHD simulation indicates that the arrival of an RD produces two time-dependent intermediate shocks (TDISs) and two slow shocks downstream of the bow shock, which propagate through the magnetosheath toward the Earth's magnetopause. An enhancement of plasma density is present throughout the TDISs and slow shocks. A plasma dynamic pressure pulse is formed in this region. In the hybrid simulation, the two TDISs are replaced by rotational discontinuities. For a bow shock with a shock normal angle $\theta_{Bn} > 45^o$, the pulse in the dynamic pressure ρV^2 causes the the total pressure $(P + B^2/2\mu_0 + \rho V^2)$ in the magnetosheath to increases by about 0-100% of the background value. The strength of the pressure pulse increases with the field rotation angle across the incident rotational discontinuity, while it decreases with the Mach number or upstream plasma beta of the bow shock. The pressure pulse propagates toward the magnetopause with nearly a constant amplitude. On the other hand, the BS/AW interaction leads to the generation of Alfven waves downstream of the bow shock, and large-amplitude dynamic pressure pulses are generated in the downstream Alfven wave. Pressure pulses impinging on the magnetopause may produce magnetic impulse events (MIEs) observed in the high-latitude ionosphere.

1. Introduction

The Earth's magnetopause is the location where solar wind mass, energy, and momentum are transferred to the magnetosphere. A variety of transient physical processes may occur at the magnetopause, including bursty magnetic reconnection resulting in flux transfer events (FTEs) [*Russell and Elphic,* 1978], riplets on the magnetopause driven by solar wind dynamic pressure pulses [*Kaufmann and Konradi,* 1969], and wavy magnetopause motion produced by the Kelvin-Helmholtz instability [*Southwood,* 1968].

Since the footprints of magnetic field lines in the outer dayside magnetosphere map to the vicinity of the dayside auroral oval, one might expect ground magnetometers located in this region to observe corresponding transient events. Indeed, *Lanzerotti et al.* [1986, 1987], *Lanzerotti* [1989], and *Glassmeier et al.* [1989] have reported examples of isolated large-amplitude (several tens of nenateslas) impulsive ($\sim$ several minutes in duration) perturbations in high-latitude ground magnetograms. *Bering et al.* [1988, 1990] have shown that impulsive perturbations in the ionospheric electric field accompany such events. Statistical studies reveal that the events are most common in the dayside ionosphere [*Glassmeier et al.,* 1989; *Lanzerotti et al,* 1991]. When chains of ground magnetograms are used, the events can frequently be interpreted in terms of antisunward moving traveling convection vortices [e.g., *Friis-Christensen et al.,* 1988].

The initial observational studies were prompted by suggestions that FTEs might produce unique small-scale ionospheric convection patterns and corresponding signatures in ground magnetograms [*Saunders et al.,* 1984; *Southwood,* 1985, 1987; *Lee,* 1986]. Theory predicts that such events would first move azimuthally under the influence of magnetic curvature forces and then

[1] College of Science, National Cheng Kung University, Tainan, Taiwan.

[2] Geophysical Institute and Department of Physics, University of Alaska, Fairbanks, Alaska.

Paper number 95JA02985.
0148-0227/96/95JA-02985$05.00

poleward under the influence of magnetosheath pressure gradients. Typical velocities would be of the order of $\sim$ 1km/s. Flow speeds and directions at the center of the events would have to be in their direction of motion. However, observations reveal that the events generally move antisunward at velocities much greater than 1km/s [*Sibeck*, 1991]. Furthermore, the events translate in a direction perpendicular to that inferred for the flows at their center [*Friis-Christensen et al.*, 1988]. A number of case studies suggest that the events are related to changes in the solar wind dynamic pressure and/or interplanetary magnetic field (IMF) orientation [*Friis-Christensen et al.*, 1988; *Sibeck et al.*, 1989; *Farrugia et al.*, 1989], and new theories have been developed along these lines [e.g., *Southwood and Kivelson*, 1990; *Glassmeier and Heppner*, 1992; *Lysak et al.*, 1994]. The effects of solar wind dynamic pressure changes on the magnetopause have also been studied by simulations of the interaction between an interplanetary tangential discontinuity and the bow shock [*Mandt and Lee*, 1991; *Wu et al.*, 1993].

Konik et al. [1994] examined statistically the IMF conditions and solar wind plasma parameters observed by IMP 8 upstream of the bow shock during magnetic impulse events observed by near cusp-latitude stations. They found that over 50% of the events are associated with substantial variations in the IMF direction (variations in B_y and B_z), while only 15%-30% of the events are accompanied by changes in the solar wind dynamic pressure. *Bering et al.* [1990] reported several magnetic impulse events (MIEs) in which the direction of the IMF changes greatly, whereas the solar wind dynamic pressure and magnetic field strength remain nearly constant. If the events are caused by pressure changes applied to the magnetosphere, such changes must be generated at the bow shock or in the magnetosheath.

In this paper, we study the generation of plasma dynamic pressure pulses due to a change in the interplanetary magnetic field orientation striking the bow shock. The interaction of an interplanetary rotational discontinuity (RD) or an Alfven wave (AW) with the bow shock is investigated. Figure 1 schematically illustrates the generation of pressure pulses in the magnetosheath by varying the IMF orientation. At time $t = 0$, the interplanetary magnetic field lines are shown by the dashed lines. Downstream of the bow shock, which is a fast shock, the magnetic field strength increases and the field lines drape in the magnetosheath. If the IMF suddenly changes to a new direction, as shown by the solid lines, the downstream magnetic field will increase in this new direction near the bow shock, and kinked field lines and associated MHD discontinuities and waves will be formed between the new and the unperturbed plasma regions in the magnetosheath as a result of the interaction between the interplanetary rotational discontinuity and the bow shock. A dynamic pressure pulse may be generated in the discontinuities and waves, as indicated by the shaded area in the magnetosheath. Propagation of the pressure pulse to the magnetopause may lead to a wavy motion of the magnetopause and generate traveling vortices and MIEs in the ionosphere. Note that the pressure pulse and twisted field lines shown in Figure 1 are transient phenomena.

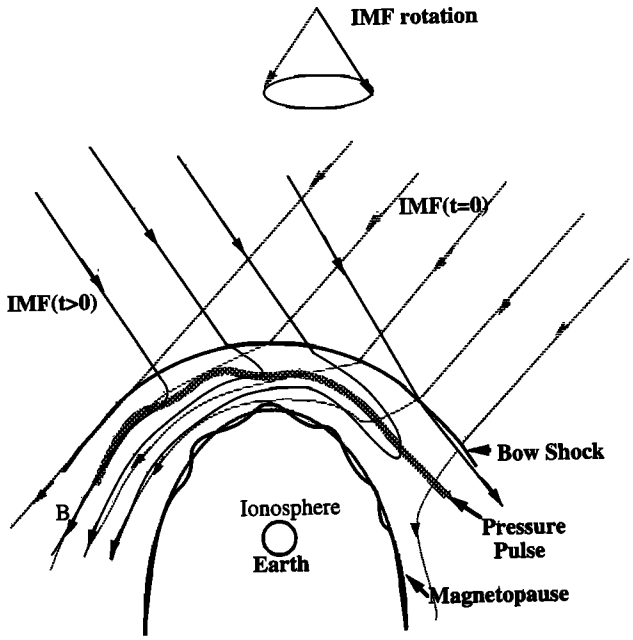

Figure 1. A schematic sketch for the generation of a dynamic pressure pulse in the magnetosheath by the variation of the interplanetary magnetic field (IMF) orientation. Note that the dynamic pressure pulse (shaded area) is a transient phenomenon.

Hassam [1978] used an ideal MHD analysis to study the transmission of Alfven waves through the bow shock. Recent MHD simulation studies by *Yan and Lee* [1994, 1995] indicate that slow-mode waves and other discontinuities can be generated in the magnetosheath by the interaction between the bow shock and various MHD discontinuities or waves in the upstream solar wind. Slow-mode structures in the magnetosheath have also been discussed by *Song et al.* [1992], *Hubert* [1994], and *Denton et al.* [1995]. In addition, the simulation study by *Yan and Lee* [1995] also indicates an enhancement of dynamic pressure in the magnetosheath. The generation and evolution of the pressure pulse in the collisionless magnetosheath plasma, however, have not been studied.

In this paper, a one-dimensional (1-D) hybrid simulation is carried out to study the interaction between an interplanetary rotational discontinuity (RD), or Alfven wave (AW), and the bow shock (BS) in collisionless plasmas. An MHD simulation of the BS/RD (BS/AW) interaction is also presented for comparison. A small resistivity is imposed in the MHD simulation to stabilize the calculation. The models used in this study are described in section 2. An analysis of the resulting dynamic pressure pulse is given in section 3. A parameter search based on the ideal MHD formulation of the Riemann problem [*Lin and Lee*, 1994] is shown in section 4. Finally, a summary of the paper is given in section 5.

2. Models of the Study

We consider three types of interplanetary magnetic field variations: a rotational discontinuity (RD), an Alfven wave pulse (AW), and an Alfven wave train. In this paper, the Alfven wave pulse is defined to have a finite spatial extent which is much longer than the rotational discontinuity but to have a field rotation angle within 360^o. The Alfven wave train contains several 360^o rotations of the magnetic field. In a plasma with an isotropic temperature, the direction of the tangential magnetic field can change arbitrarily across the rotational discontinuity, while the magnetic field strength and plasma density and pressure remain unchanged. The change of velocity across the rotational discontinuity should obey the Walen relation

$$\Delta \mathbf{V} = \pm \Delta \mathbf{B}/\sqrt{\mu_0 \rho} \tag{1}$$

where $\Delta \mathbf{V}$ is the variation of flow velocity across RD, $\Delta \mathbf{B}$ is the change of magnetic field, ρ is the plasma density, and the positive (negative) sign is applied if the normal incident velocity is parallel (antiparallel) to the normal component of magnetic field.

In the next section, we carry out 1-D MHD simulations and hybrid simulations to solve the Riemann problem associated with the BS/RD (BS/AW) interaction. All the dependent variables are functions of the spatial coordinate x and time t only, where $\mathbf{x}$ is along the normal direction of shocks or discontinuities. In the 1-D system, the normal component of the magnetic field $B_n = B_x < 0$ is a constant. The tangential component of the magnetic field upstream and downstream of the BS is assumed to be in the z direction, and the tangential magnetic field at the RD is in the yz plane.

The MHD simulation solves the set of MHD equations with a small resistivity η, which is imposed to stabilize the calculation. The basic equations are

$$\frac{\partial \rho}{\partial t} = -\nabla \cdot (\rho \mathbf{V}) \tag{2}$$

$$\frac{\partial (\rho \mathbf{V})}{\partial t} = -\nabla \cdot [(\rho \mathbf{V}\mathbf{V}) + (P + \frac{B^2}{2\mu_0})\mathbf{I} - \frac{1}{\mu_0}\mathbf{B}\mathbf{B}] \tag{3}$$

$$\frac{\partial \mathbf{B}}{\partial t} = \nabla \times (\mathbf{V} \times \mathbf{B}) \tag{4}$$

$$\frac{\partial \epsilon}{\partial t} = -\nabla \cdot \mathbf{S} \tag{5}$$

The energy flux $\mathbf{S}$ and the energy density ϵ are defined as

$$\mathbf{S} = (\epsilon + P + \frac{B^2}{2\mu_0})\mathbf{V} - \frac{1}{\mu_0}(\mathbf{B} \cdot \mathbf{V})\mathbf{B} + \eta \mathbf{J} \times \mathbf{B} \tag{6}$$

$$\epsilon = \frac{1}{2}\rho V^2 + \frac{B^2}{2\mu_0} + \frac{P}{\gamma - 1} \tag{7}$$

where P is the thermal pressure, μ_0 is the permeability in free space, and the current density $\mathbf{J}$ is given by

$$\mathbf{J} = \frac{1}{\mu_0}\nabla \times \mathbf{B} \tag{8}$$

The polytropic index is chosen as $\gamma = 5/3$. In the 1-D simulation, we set $\partial/\partial y = \partial/\partial z = 0$.

In our study, the initial RD (or AW) propagates toward the BS from upstream along the $-\mathbf{x}$ direction, as sketched in the top plot of Figure 2. Initially, the BS is located at $x = x_F$. The rotational discontinuity is at $x = x_R$, propagating in the upstream solar wind with the intermediate-mode speed, which equals the normal component of Alfven velocity. The initial BS and RD divide the 1-D system into three regions: Region 0 downstream of the RD, Region 1 upstream of the RD and upstream of the BS, and Region 2 downstream of the BS. Note that the Earth is located on the left in Figure 2. Once the rotational discontinuity reaches the bow shock, it in general cannot simply penetrate through the bow shock without generating other discontinuities. This is due to the change in the Alfven speed across the bow shock, which is caused by the changes in the magnetic field and plasma density. In order to match the plasma flow velocity from the initial Region 2 value to the Region 0 value, the field rotation angle of the initial RD will be modified in the downstream region of the bow shock, and other wave modes will be generated. According to the fluid theory of discontinuity/discontinuity (or shock/discontinuity) interaction [e.g., *Landau and Lifshitz,* 1959], the original RD/BS system evolves to form a new set of MHD discontinuities at $t > 0$. The initial value problem associated with the evolution of an initial current sheet is called the Riemann problem [e.g., *Jeffrey and Taniuti,* 1964; *Lin and Lee,* 1994]. In the ideal MHD, fast shocks, rotational discontinuities, slow shocks, and a contact discontinuity may be formed as a result of the discontinuity/discontinuity interaction, as shown in the bottom plot of Figure 2. Some of the MHD shocks which are generated by the BS/RD interaction may correspond to a dynamic pressure pulse.

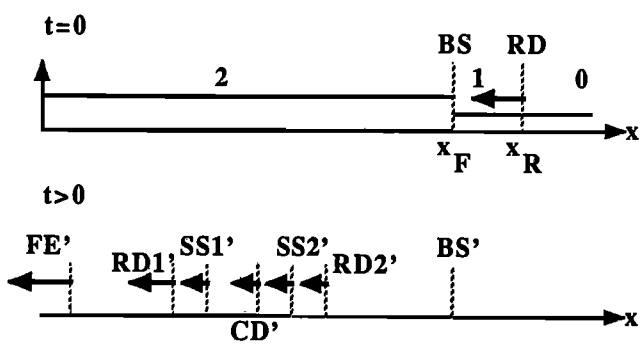

Figure 2. An illustration of the Riemann problem associated with the BS/RD interaction. The initial rotational discontinuity (RD) propagates from the interplanetary space toward the bow shock (BS) at $t = 0$, while RD and BS divide the system into three uniform regions, Regions 0, 1, and 2. As RD reaches BS, the system evolves into seven discontinuities and waves. The fast expansion wave FE′, rotational discontinuity RD1′, slow shock SS1′, contact discontinuity CD′, slow shock SS2′, and rotational discontinuity RD2′ propagate toward the magnetopause (left side) in the downstream region of the bow shock BS′.

In resistive MHD, steady rotational discontinuities cannot exist and are replaced by intermediate shocks for an 180° magnetic field rotation or time-dependent intermediate shocks (TDISs) for an arbitrary field rotation angle. Across the TDIS, the plasma density increases. The normal component of plasma flow velocity is superintermediate, i.e., greater than the intermediate-mode speed, in the upstream region and subintermediate, i.e., less than the intermediate-mode speed, in the downstream region. The strength of the TDIS decreases and the width increases as $\sqrt{t}$. As $t \to \infty$, the TDIS evolves toward a rotational discontinuitylike structure with an infinite thickness [*Wu and Kennel,* 1992; *Lin et al.,* 1992]. In hybrid simulations of space plasma, however, the steady rotational discontinuity may exist [e.g., *Lee et al.,* 1989; *Richter and Scholer,* 1989; *Goodrich and Cargill,* 1991; *Lin and Lee,* 1993], and the TDIS evolves quickly to a steady rotational discontinuity [*Lin and Lee,* 1993]. In the solar wind, rotational discontinuities and Alfven waves are frequently observed by spacecraft [e.g., *Burlaga,* 1969].

The ratios of downstream to upstream quantities at the initial bow shock are determined by the MHD Rankine-Hugoniot jump relations of a fast shock. The initial profiles for the z component of the magnetic field, the strength of the tangential magnetic field component B_t, the plasma density ρ, and the temperature T are given by

$$B_z(x) = \begin{cases} \frac{1}{2}(B_{z1} + B_{z2}) + \frac{1}{2}(B_{z1} - B_{z2}) \times \\ \quad \tanh[(x - x_F)/\delta_F], \text{ if} x \le x_c; \\ \frac{1}{2}(B_{z0} + B_{z1}) + \frac{1}{2}(B_{z0} - B_{z1}) \times \\ \quad \tanh[(x - x_R)/\delta_R], \text{ if} x \ge x_c. \end{cases} \quad (9)$$

$$B_t(x) = \begin{cases} B_z(x), & \text{if } x \le x_c; \\ B_{t0}, & \text{if } x \ge x_c. \end{cases} \quad (10)$$

$$\rho(x) = \begin{cases} \frac{1}{2}(\rho_1 + \rho_2) + \frac{1}{2}(\rho_1 - \rho_2)\tanh[(x - x_F)/\delta_F], \\ \qquad \text{if} x \le x_c; \\ \rho_0, \\ \qquad \text{if} x \ge x_c. \end{cases} \quad (11)$$

$$T(x) = \begin{cases} \frac{1}{2}(T_1 + T_2) + \frac{1}{2}(T_1 - T_2)\tanh[(x - x_F)/\delta_F], \\ \qquad \text{if} x \le x_c; \\ T_0, \\ \qquad \text{if} x \ge x_c. \end{cases} \quad (12)$$

where δ_F and δ_R are the transition widths at x_F (fast shock) and x_R (rotational discontinuity), respectively, $x_c = (x_R + x_F)/2$, $B_{t0} = (B_{y0}^2 + B_{z0}^2)^{1/2}$, and the subscripts 0, 1, and 2 indicate quantities in Regions 0, 1, and 2, respectively. Note that $\rho_0 = \rho_1$, $T_0 = T_1$, and $B_{t0} = B_{t1}$ across an RD. At the bow shock, $B_{y1} = B_{y2} = 0$ is assumed.

The initial profile of normal flow velocity, which is a constant across an RD, is given by

$$V_x(x) = \frac{1}{2}(V_{x0} + V_{x2}) + \frac{1}{2}(V_{x0} - V_{x2})\tanh[(x - x_F)/\delta_F] \quad (13)$$

The tangential velocity across the RD obeys the Walen relation (1). The simulation is performed in a frame moving with the initial bow shock. We choose the frame in which the magnitude of tangential flow velocity remains constant across the RD, so that, initially, the dynamic pressure ρV^2 is a constant everywhere upstream of the bow shock. In fact, for the bow shock with an Alfven Mach number $M_A > 5$, ρV^2 is nearly a constant across the initial RD even in the normal incident frame of the bow shock, in which the flow velocity just upstream of the bow shock is along the normal direction. The dynamic pressure pulse generated in the normal incident frame of the bow shock is much larger than that in the frame of our simulation.

For cases of BS/AW interaction, a sinusoidal spatial variation in B_y and B_z is assumed at the initial Alfven wave. The velocity, density, and magnetic field strength at AW satisfy

$$\delta \mathbf{V}(x) = \pm \delta \mathbf{V}_A(x) \quad (14)$$

$$\delta \rho(x) = 0 \quad (15)$$

$$\delta B(x) = 0 \quad (16)$$

The MHD simulation code used in this study is described by *Yan and Lee* [1995]. A Runge-Kutta scheme with a fourth-order accuracy in time and a second-order accuracy in space is used to integrate the MHD equations. A free boundary condition is used. A total of 2000 grid points are used in the simulation domain. The resistivity is chosen to be $\eta = 10^{-5}$ when normalized to $(\mu_0 L_x / B_0^2)$, where L_x is the length of the simulation domain. Note that in resistive MHD, the rotational discontinuity RD diffuses and should be replaced by a TDIS. We set the initial rotational discontinuity to be at a position very close to the bow shock to avoid the decay because of a finite resistivity in the MHD simulation. The results from using a rotational discontinuity and a weak TDIS show almost no difference.

The hybrid code used in this study is that of *Swift and Lee* [1983]. In this model, ions are treated as individual particles moving in a corresponding electromagnetic field, and electrons are treated as a massless fluid. Charge neutrality is assumed in the calculation. In the simulation, the length per cell is $0.158\lambda_0$, where the ion inertial length upstream of the bow shock $\lambda_0 = c/\omega_{pi0}$, c is the speed of light, and ω_{pi0} is the ion plasma frequency upstream of the bow shock. The system length used in our study is 3000-4000 cells. Two buffer zones are located at the two ends of the simulation domain. The hybrid simulation results shown in this paper are only for the central part of the whole simulation domain, ranging from $x = 0$ to $x = L_x$, where $L_x = 320\text{-}450\lambda_0$. The ion number density per cell, N, upstream of the bow shock is $N_0 = 25\text{-}50$. The bow shock and initial rotational discontinuity have a half width of $2\text{-}4\lambda_0$. The initial position of the bow shock is at $x_F = 0.6L_x$, and that of the rotational discontinuity is at $x_R = 0.8L_x$.

The hybrid simulation results shown in this paper are only for quasi-perpendicular fast shocks. The hybrid simulations which involve a quasi-parallel shock are more complicated [e.g., *Burgess,* 1989; *Lyu and Kan,* 1990; *Scholer and Terasawa,* 1990]. For cases involving

a quasi-perpendicular shock, the hybrid simulation has also been performed for the situation in which the initial bow shock and rotational discontinuity are those which have been simulated individually for a long time so that the collisionless structure of the discontinuities has developed before they are introduced in the simulation system of BS/RD interaction. The resulting dynamic pressure pulses are nearly the same as in the cases with initial profiles given by (13)-(16).

3. Generation of the Dynamic Pressure Pulse

The simulation results for our four cases are shown in this section. In Case 1, the BS, which is a fast shock, interacts with an interplanetary RD across which the tangential magnetic field rotates by an angle of 160°. The structure of the fast shock alone is also shown for comparison. In Case 2, the initial rotational discontinuity in Case 1 is replaced by an Alfven wave pulse. Case 3 is for the interaction between a fast shock and an Alfven wave pulse with a 360° rotation in magnetic field. In Case 4, the fast shock interacts with an Alfven wave train which contains three 360° rotations of magnetic field.

3.1. Case 1: Interaction Between the Bow Shock and a Rotational Discontinuity

In Case 1, the shock normal angle of the initial fast shock is $\theta_{Bn} = 50°$, the thermal to magnetic pressure ratio in the upstream region of the fast shock is $\beta_0 = 0.5$, and the Alfven Mach number of the fast shock is $M_A \equiv V_{n0}/V_{A0} = 6$, where V_{n0} is the upstream normal flow speed and $V_{A0} = B_0/\sqrt{\mu_0\rho_0}$ is the Alfven speed in the upstream. The initial rotational discontinuity propagates toward the bow shock in the upstream solar wind, and the rotation angle of the magnetic field across the incoming rotational discontinuity is $\Delta\Phi = 160°$.

Figure 3 shows MHD simulation results for Case 1. Spatial profiles of the magnetic field component B_z, plasma density ρ, and dynamic pressure ρV^2 based on the total velocity are plotted in Figure 3a for a time series from $t = 0$ to $t = 0.37t_A$, where $t_A = L_x/V_{A0}$. Note that the x component of the flow velocity V_x may not be along the normal at the magnetopause, and the plasma flow parallel to the bow shock front may have a normal component at the magnetopause, which contributes to the dynamic pressure at the magnetopause. The dynamic pressure pulse may cause the magnetopause to move inward.

Seven discontinuities are generated by the interaction between the initial BS and RD. They are, from the Earth (left) side, a weak fast expansion wave (FE′ in Figure 3a), a time-dependent intermediate shock (TDIS1′), a slow shock (SS1′), a contact discontinuity (CD′), a slow shock (SS2′), a time-dependent intermediate shock (TDIS2′), and a fast shock (BS′). Since the propagation speeds of TDIS1′ and SS1′ are very similar in this case, these two discontinuities are not separated in Figure 3a. Similar results are found for TDIS2′ and SS2′. The strength and position of the fast shock BS′ are almost the same as those of the initial bow shock. The normal component of the flow velocity is superfast upstream of the fast shock and subfast and superintermediate downstream [e.g., *Landau and Lifshitz*, 1960]. The other six discontinuities are convected downstream of the bow shock BS′ in the magnetosheath. The structure TDIS1′/SS1′ or TDIS2′/SS2′ evolves toward a 2-3 time-dependent intermediate shock, whose upstream normal inflow speed is superintermediate and subfast and downstream normal flow speed is superslow and subintermediate, and a quasi-steady slow shock at a later time [*Lin et al.*, 1992]. Relative to the contact discontinuity CD′, which has a zero propagation speed in the plasma frame [*Landau and Lifshitz*, 1960], TDIS1′ and SS1′ propagate to the left side and TDIS2′ and SS2′ to the right side. Nevertheless, since the normal flow convection speed downstream of the fast shock is superintermediate and the wave speeds of time-dependent intermediate shocks and slow shocks in Case 1 are very close to the local intermediate speed, the discontinuities TDIS1′, SS1′, CD′, SS2′, and TDIS2′ propagate toward the magnetopause, which is to the left along the x axis, relative to the bow shock BS′. The fast expansion wave FE′ propagates rapidly toward the magnetopause. In this case, FE′ is very weak, as seen from slight decreases in ρ and ρV^2 from upstream to downstream.

A dynamic pressure pulse is formed downstream of the bow shock, as seen from the ρV^2 profile in Figure 3a. This pressure pulse is present throughout TDIS1′, SS1′, CD′, SS2′, and TDIS2′ and propagates with these discontinuities toward the magnetopause. The distance between the discontinuities and thus the width of the pressure pulse broaden with time.

Figure 3b shows a hodogram of the tangential magnetic field and spatial profiles of B_y, B_z, B^2, ρ, P, V_y, V_z, ρV^2, the total pressure $P_x \equiv (P + B^2/2\mu_0 + \rho V_x^2)$ associated with V_x, and the total pressure $P_{\rm tot} \equiv (P + B^2/2\mu_0 + \rho V^2)$ associated with the total velocity V at $t = 0$ and $0.32t_A$. The pressure terms are normalized to $P_{B0} \equiv B_0^2/2\mu_0$. The discontinuities TDIS1′ and SS1′ are nearly coincident at this time. The tangential magnetic field varies through a large angle across TDIS1′/SS1′, as shown in the hodogram and magnetic field profiles in Figure 3b. The magnetic field strength decreases, while the plasma density and thermal pressure increase across the structure TDIS1′/SS1′. The flow velocity V_z is enhanced across the structure. The profiles for the plasma density, pressure, and velocity at TDIS2′/SS2′ are very similar to those at TDIS1′/SS1′. The magnetic field changes across a much smaller angle at TDIS2′/SS2′ than that at TDIS1′/SS1′, as seen from the hodogram. Note that in the BS/RD interaction, the initial RD has almost no influence on the bow shock strength and position, but the magnetic field direction at the bow shock is changed to be in the direction of the initial Region 0 field. The initial RD is modified in the interaction. The time-dependent intermediate shock TDIS1′ evolves toward a rotational discontinuity

with a field rotation angle much closer to the initial RD than TDIS2′ does.

Across the contact discontinuity CD′, the plasma density changes, but the magnetic field, pressure, and flow velocity are conserved. A plateau of density and pressure enhancement is formed between TDIS1′ and TDIS2′.

In general, at slow or time-dependent intermediate shocks, the sum of the thermal and magnetic pressure $(P + B_0^2/2\mu_0)$ remains nearly a constant. In the region of density enhancement in Case 1, the decrease of the magnetic pressure $(B^2/2\mu_0)$ is nearly equal to the increase of the thermal pressure P, and $(P + B_0^2/2\mu_0)$ is therefore nearly a constant. The x component of the flow velocity is nearly constant throughout the discontinuities downstream of the bow shock. The variation of the dynamic pressure associated with the normal flow speed, ρV_x^2, is also small.

The dynamic pressure ρV^2, however, increases by $\sim$ 100% across TDIS1′/SS1′. It increases by $\sim$ 95% across TDIS2′/SS2′. As a result, the total pressure $P_{\rm tot}$ increases by $\sim$ 40%, as shown in Figure 3b. The dynamic pressure pulse propagates to the magnetopause with a speed of $\sim 2V_{A0}$.

The simulation result indicates little change in the velocity along the Sun-Earth line. On the other hand, a substantial deflection of the flow in the y-z direction is present as a result of the arrival of an interplanetary rotational discontinuity. The deflection of the flow is proportional to the rotation angle of the tangential magnetic field across the rotational discontinuity, which can be as large as the Alfven speed in the background magnetosheath. As the dynamic pressure approaches the magnetopause, it may be deflected and slowed, and an enhanced thermal and magnetic pressure is applied to the magnetosphere. The arrival of the pressure pulse at the magnetopause will change the location of the magnetopause positions away from the subsolar point, in particular along the flanks where the magnetopause lies normal to the flow deflections. Note that the 2-D effects in the BS/RD interaction are not discussed in this paper, which may also be important in the study of the dynamic pressure pulse.

It should be mentioned that the amplitude of the dynamic pressure pulse obtained from the MHD simulation is smaller than that from the hybrid simulation, as will be shown below. This is due to the presence of the time-dependent intermediate shock, across which

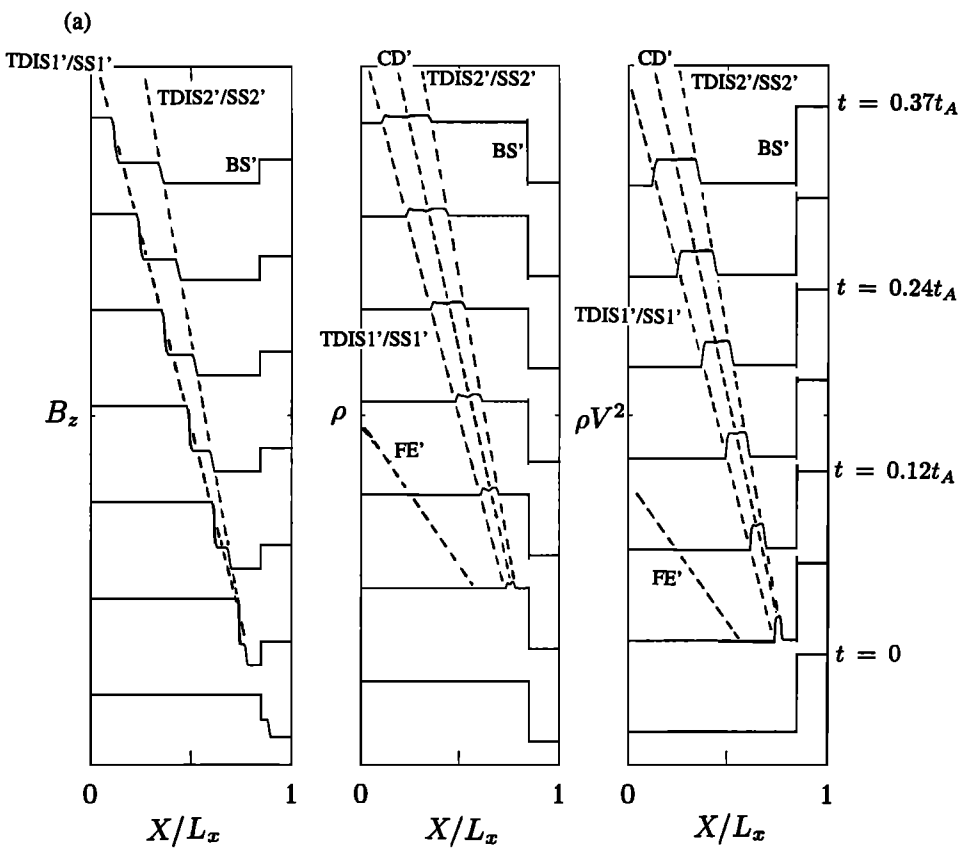

Figure 3. MHD simulation results of Case 1, in which $\theta_{Bn} = 50°$, $M_A = 6$, $\beta_0 = 0.5$, and $\Delta\Phi = 160°$. (a) Spatial profiles of B_z, ρ, and ρV^2 in a time series from $t = 0$ to $t = 0.37t_A$. Here TDIS1′ and TDIS2′ indicate two time-dependent intermediate shocks. The discontinuities TDIS1′ and SS1′ (TDIS1′ and SS2′) have not been separated. (b) The hodogram of tangential magnetic field and spatial profiles of B_y, B_z, B^2, ρ, P, V_y, V_z, ρV^2, P_x, and $P_{\rm tot}$ at $t = 0$ and $t = 0.32t_A$, where $P_x \equiv (P + B^2/2\mu_0 + \rho V_x^2)$ and $P_{\rm tot} \equiv (P + B^2/2\mu_0 + \rho V^2)$. The pressure terms are normalized to $P_{B0} \equiv B_0^2/2\mu_0$.

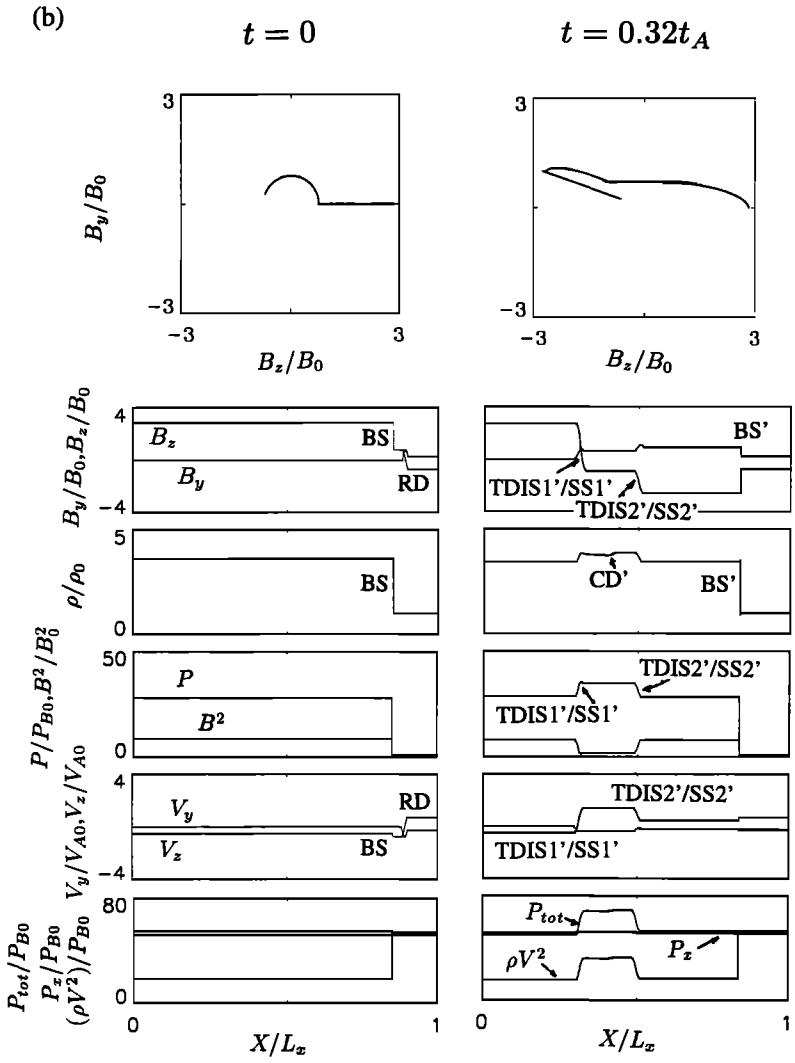

Figure 3. (Continued)

the magnetic field strength decreases, and thus the variation of the tangential flow velocity is not as large as that across a rotational discontinuity, which appears in the hybrid simulation.

The hybrid simulation results of Case 1 are given below. Figure 4 shows the hodogram of tangential magnetic field and spatial profiles of B_y, B_z, B^2, ion number density N, thermal pressure parallel to the magnetic field $P_{\|}$ (solid line), perpendicular pressure $P_{\perp}$ (dotted line), parallel temperature $T_{\|}$ (solid line), perpendicular temperature $T_{\perp}$ (dotted line), V_x, V_y, V_z, dynamic pressure $m_i N V^2$, pressure $P_x \equiv (P + B^2/2\mu_0 + N m_i V_x^2)$, and total pressure $P_{\rm tot} \equiv (P + B^2/2\mu_0 + N m_i V^2)$ at $t = 0$ and $t = 55\Omega_0^{-1}$, where m_i is the ion mass, $P = (P_{\|} + 2P_{\perp})/3$ and Ω_0 is the ion cyclotron frequency upstream of the bow shock. Note that the pressure terms in Figure 4 are normalized to $P_{B0} = B^2/2\mu_0$. The initial bow shock is located at $x = 175\lambda_0$, and the rotational discontinuity is at $x = 205\lambda_0$. For comparison, Figure 5 shows the simulation of the bow shock alone at $t = 55\Omega_0^{-1}$ for the same initial profile of the shock but without an interaction with any rotational discontinuity. Now there is no significant pressure pulse downstream of the bow shock.

For the simulation shown in Figure 4, the initial rotational discontinuity reaches the bow shock at $t \simeq 8\Omega_0^{-1}$. At $t = 55\Omega_0^{-1}$, a rotational discontinuity, RD1′, with a large magnetic field rotation from "a" to "b" propagates downstream of the bow shock, as shown in the field profiles and hodogram. The field rotation angle across RD1′ is almost the same as the initial angle $\Delta\Phi$. The small rotational discontinuity (time-dependent intermediate shock) in the MHD simulation cannot be clearly identified in the hybrid simulation. The bow shock is located between an upstream point "f" and a downstream point "e". The many fluctuations just downstream of the bow shock are associated with the collisionless structure of the bow shock. Two slow shocks, SS1′ from "b" to "c" and SS2′ from "d" to "c," propagate behind RD1′. The magnetic field strength decreases across the slow shock. The contact discontinuity cannot be identified because of the ion mixing along the magnetic field

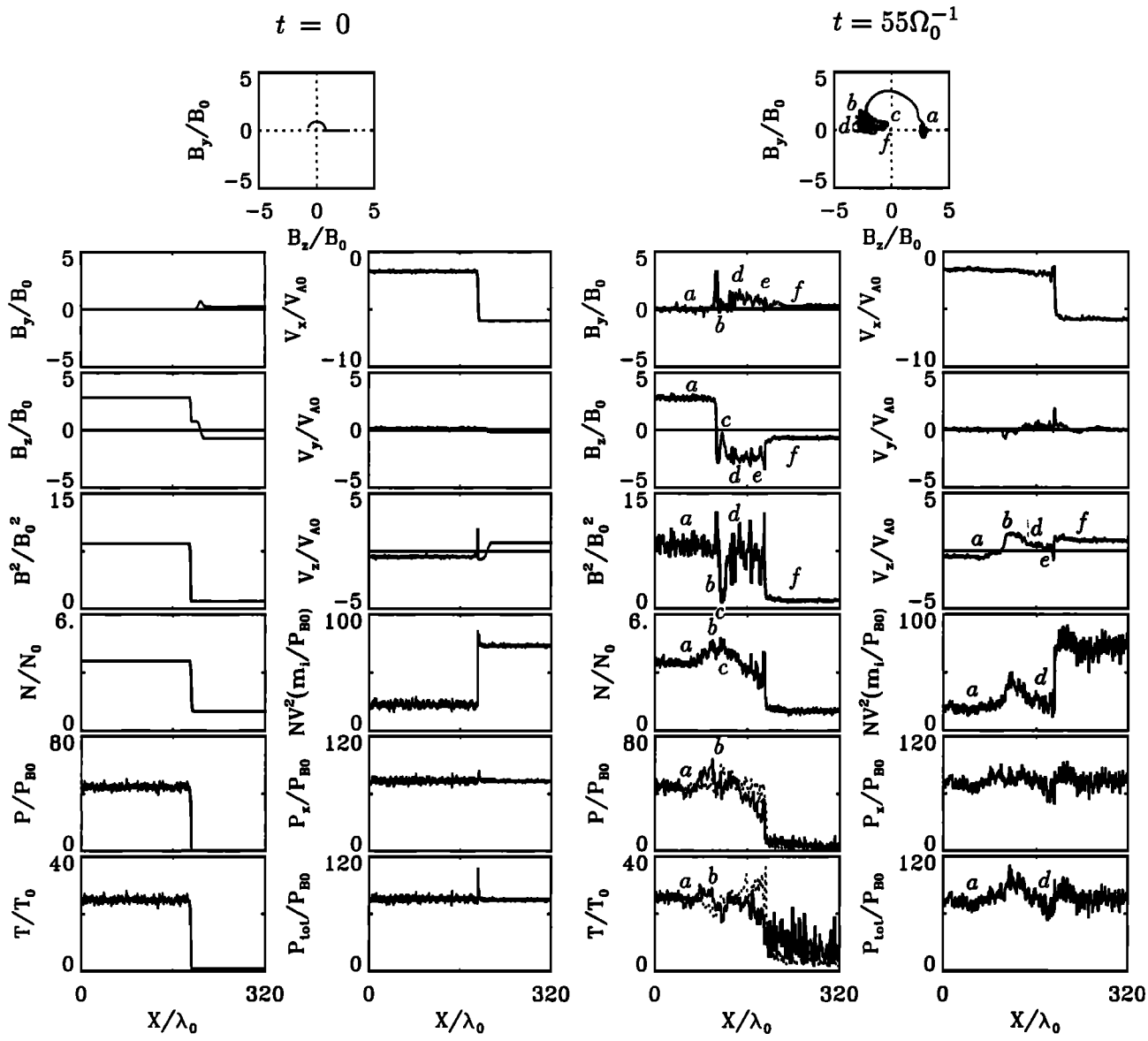

Figure 4. Hybrid simulation results of Case 1. The hodogram of tangential magnetic field and spatial profiles of B_y, B_z, B^2, N, $P_{\|}$ (solid line), $P_{\perp}$ (dotted line), $T_{\|}$ (solid line), $T_{\perp}$ (dotted line), V_x, V_y, V_z, NV^2, P_x, and $P_{\rm tot}$ are shown for $t = 0$ and $t = 55\Omega_0^{-1}$.

[*Lin and Lee*, 1993], and the small rotational discontinuity (time-dependent intermediate shock) in the MHD simulation cannot be clearly seen in the hybrid simulation. The weak fast expansion wave, as shown in the MHD simulation, can hardly be identified.

The parallel pressure $P_{\|}$ increases across RD1′, while the perpendicular pressure is nearly constant, as shown in Figure 4. A pressure anisotropy with $\alpha_d > \alpha_u$ is observed, where $\alpha = (\beta_{\|} - \beta_{\perp})/2$, and the subscripts "u" and "d" indicate, quantities in the upstream and downstream regions of RD1′, respectively. Since $N(1 - \alpha)$ is conserved across a rotational discontinuity, the density increases across the discontinuity [e.g., *Lin and Lee*, 1993]. The parallel temperature increases, while the perpendicular temperature decreases. An ion density enhancement of 30% is found across RD1′. The density also increases across SS1′ or SS2′ from upstream to downstream, as does the perpendicular pressure. The total density increase across RD1′ and SS1′ is larger than that in the MHD simulation due to the pressure anisotropy. In the region of the density enhancement, the normal flow velocity remains almost constant, and the total pressure P_x associated with V_x increases about 10% of the background value.

On the other hand, a large variation in the tangential flow velocity is present from "a" to "d," as seen in the V_z profile of Figure 4. A large dynamic pressure pulse associated with the total velocity is formed downstream of the bow shock, as shown in the NV^2 profile, which is a measure of the dynamic pressure $m_i NV^2$. Correspond-

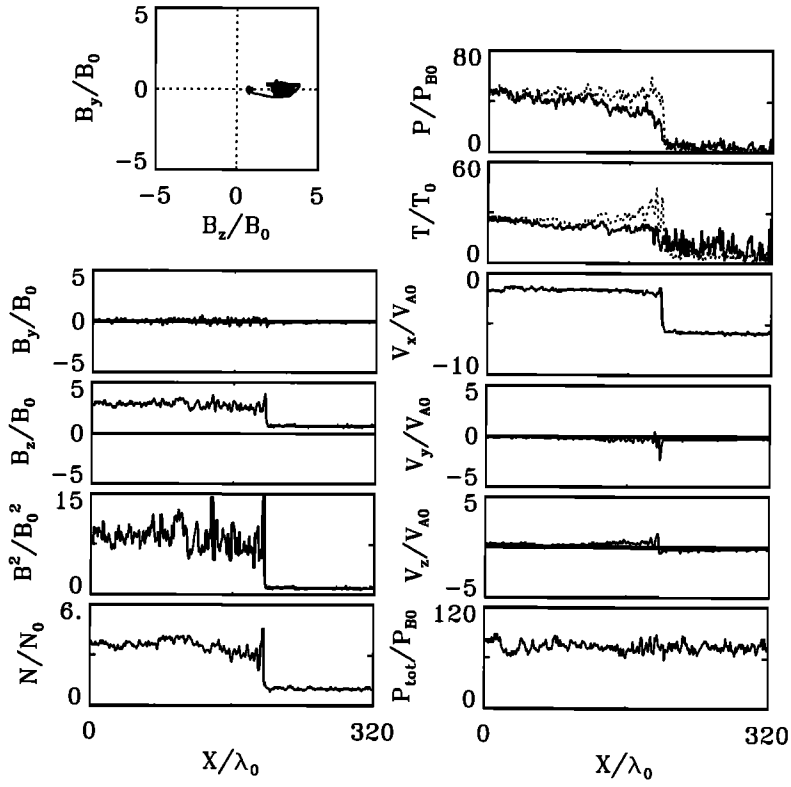

Figure 5. Hybrid simulation of the fast shock in Case 1: the magnetic field hodogram and spatial profiles of various quantities at $t = 55\Omega_0^{-1}$.

ingly, the total pressure P_{tot} increases by nearly 50% of the background value in the magnetosheath. Note that in the bow shock's normal incident frame, the increase of P_{tot} is nearly 100%. It is found that the pressure pulse propagates to the magnetopause with nearly constant amplitude.

We have also run the case in which the initial rotational discontinuity propagates toward the Sun in the solar wind frame. The initial RD, however, still moves toward the bow shock because of the superfast plasma flow in the upstream. The simulation result is similar to that shown in Figure 4, except that the resulting rotational discontinuity with a large magnetic field rotation exists in the trailing part of the pressure pulse.

The hybrid simulation has also been performed for an initial bow shock with $\theta_{Bn} = 60^o$, 70^o, and 80^o and for $M_A = 3$, 4, 5, and 7. The results are qualitatively similar to that of Case 1. In addition, we have also run the simulation for the cases in which the initial RD has a reversed field rotation. The resulting pressure pulse is not very different from that in Case 1.

3.2. Cases 2 and 3: Interaction Between the Bow Shock and an Alfven Wave Pulse

In Case 2, the initial bow shock is the same as that in Case 1, while the incident rotational discontinuity is replaced by a sinusoidal Alfven wave pulse with a large spatial extent. The rotation angle of magnetic field through the Alfven wave is set to be 160^o, the same as in Case 1.

The MHD simulation result of Case 2 is very similar to that of Case 1, except that the TDISs and slow shocks are replaced by the corresponding compressional waves. The wavelengths of the resulting waves, however, are much shorter than that of the incident wave.

In the hybrid simulation, the spatial length of the incident Alfven pulse is chosen to be $65\lambda_0$. The magnetic field hodogram and spatial profiles of physical quantities at $t = 55\Omega_0^{-1}$ are shown in Figure 6. A rotational discontinuity (Alfven wave) is present in the magnetosheath, ranging from "a" to "b." Compared to the results in Case 1, the thickness of the rotational discontinuity is much larger. In addition, no clear slow shocks can be identified in the hybrid simulation of Case 2. The bow shock is located between "d" and "c." Similar to Case 1, an ion density enhancement and a dynamic pressure pulse are present downstream of the bow shock. The total pressure P_{tot} increases by nearly 50% from the background value at the resulting rotational discontinuity, and the pressure P_x increases by $\sim 15\%$.

Figure 7 shows spatial profiles of B_z, N, and NV^2 in a time sequence from $t = 0$ to $t = 65\Omega_0^{-1}$. After the interaction between the bow shock and the incoming Alfven wave pulse, the resulting pressure pulse propagates toward the Earth with a nearly constant amplitude. In addition, the strength of the density pulse also remains constant. As the pressure pulse propagates to the mag-

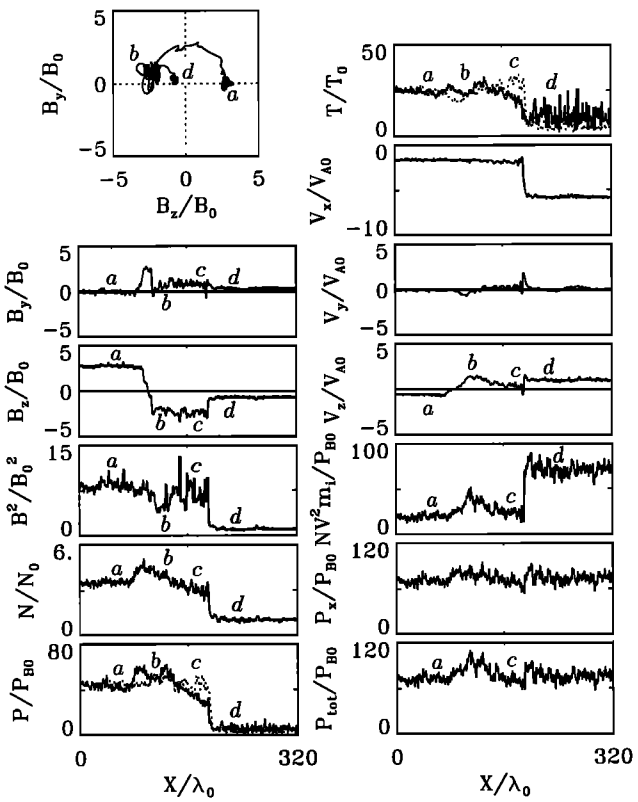

Figure 6. Hybrid simulation results of Case 2, in which the initial rotational discontinuity in Case 1 is replaced by an Alfven wave with $\Delta\Phi = 160^o$.

netopause, it also broadens along the normal direction, as shown in Figure 7. The expansion speed of each end of the pressure pulse relative to the center is nearly the intermediate-mode speed $C_{I2} = B_n/\sqrt{\mu_0\rho_2}$. The center of the pressure pulse propagates toward the magnetopause with the convection speed V_{n2} of the magnetosheath flow.

The profiles obtained from our simulation can be regarded as time lines for an observing satellite. For a solar wind plasma with an ion number density $N_0 = 5\text{cm}^{-3}$ and an IMF $B_0 = 5\text{nT}$, the Alfven speed $V_{A0} \simeq 50\text{km/s}$. The normal component of the plasma inflow velocity upstream of the bow shock is thus nearly 300km/s for $M_A = 6$, and the normal component of the downstream flow velocity is $V_{n2} \simeq 120\text{km/s}$. Therefore the time for the center of the pressure pulse to reach the magnetopause from the bow shock is $t_2 \simeq R_0/V_{n2} \simeq 3.5\text{min}$, where $R_0 \simeq 4R_e$ is the distance between the bow shock and the magnetopause. The expansion speed for each end of the pressure pulse relative to the center is nearly $C_{I2} \simeq 20\text{km/s}$ for $\theta_{Bn} = 50^o$. Thus the width of the pressure pulse is $\Delta L \simeq 8600\text{km}$ as it reaches the magnetopause. Therefore the time duration of the pressure pulse at the magnetopause is $\Delta t \simeq \Delta L/V_{n2} \simeq 1.2\text{min}$. Note that while the pressure pulse approaches the magnetopause, it may be slowed down and steepened, and the width of the pulse may be reduced.

Next, we present Case 3, in which the initial Alfven wave in Case 2 is replaced by an Alfven wave pulse

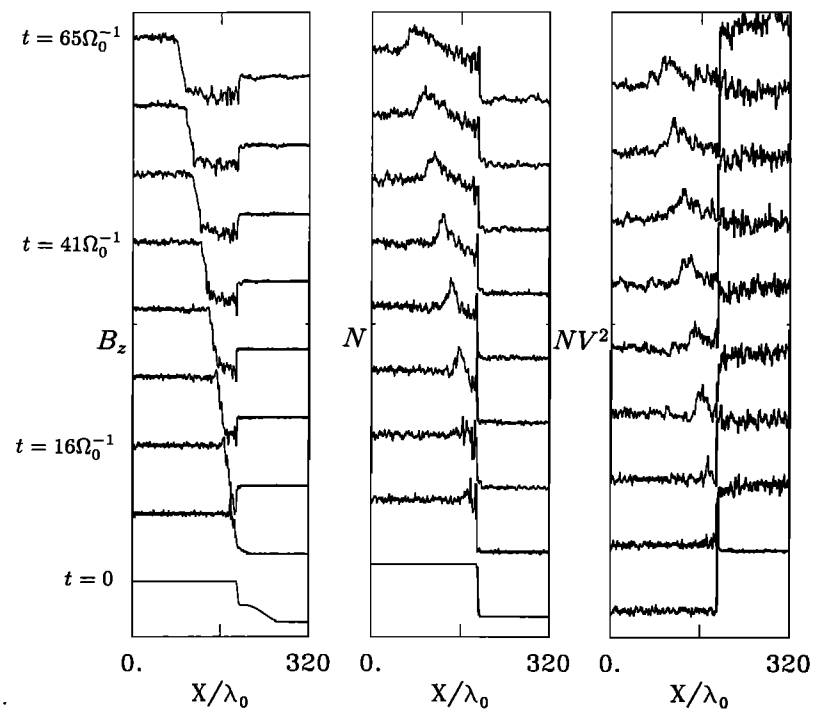

Figure 7. Spatial profiles of B_z, N, and NV^2 of Case 2 in a time sequence from $t = 0$ to $t = 65\Omega_0^{-1}$. The dynamic pressure pulse propagates toward the magnetopause (left side) with a nearly constant amplitude.

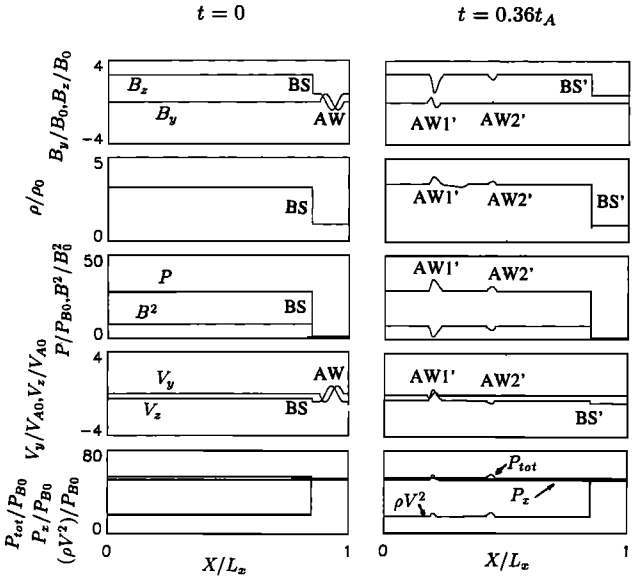

Figure 8. MHD simulation results of Case 3, in which the incident Alfven wave has a 360° field rotation and the Mach number of the bow shock $M_A = 4$.

with a 360° field rotation. The Alfven Mach number of the initial bow shock is assumed to be $M_A = 4$, and the shock normal angle and upstream plasma beta are $\theta_{Bn} = 50°$ and $\beta_0 = 0.5$, respectively. In the MHD simulation, the wavelength of the initial Alfven wave is assumed to be 200 grid points. Figure 8 shows the spatial profiles of physical quantities at $t = 0.36t_A$ from the MHD simulation. The initial profiles are shown on the left side of Figure 8. At $t = 0.36t_A$, two intermediate waves AW1′ and AW2′ are present downstream of the bow shock, as shown in Figure 8. An entropy wave exists between AW1′ and AW2′, through which the density varies but magnetic field and pressure are conserved. In the transition region of each of the two intermediate waves, the magnetic field dips and the plasma density and pressure have a peak. The flow velocity oscillates with the magnetic field. A dynamic pressure pulse is formed associated with each intermediate wave, and the pulse in the leading wave has a larger amplitude. In the MHD simulation, the strengths of the pressure pulses are not large.

Figure 9 shows the hybrid simulation results for Case 3 at $t = 70\Omega_0^{-1}$. The wavelength of the initial Alfven pulse is assumed to be $110\lambda_0$. The profiles of various quantities at $t = 0$ are also shown. At $t = 70\Omega_0^{-1}$, the bow shock is located between "d" and "c." Only one large-amplitude Alfven wave pulse is present downstream of the bow shock, ranging from "a" to "b." In the transition region of this large Alfven wave, the ion density has a peak and the magnetic pressure decreases. The maximum density enhancement is about 55%. A large pressure pulse is present in the NV^2 profile, as shown in Figure 9. The increase in the total pressure $P_{\rm tot}$ at the leading edge is nearly 50% of the background value.

3.3. Interaction Between the Bow Shock and an Alfven Wave Train

The hybrid simulation results of Case 4 at $t = 110\Omega_0^{-1}$ are shown in Figure 10. In Case 4, an initial Alfven wave train with three 360° field rotations, which correspond to three wavelengths, is incident on the bow shock. The results shown here are obtained in the normal incident frame of the bow shock. At $t = 110\Omega_0^{-1}$, three large-amplitude rotations of the magnetic field are present in the magnetosheath, as seen in the field profiles and hodograms in Figure 10. The average ion density in the field rotation region is ~ 27% higher than the background. In addition, there are three large-amplitude pulses of the dynamic pressure NV^2 associated with the three field rotations downstream of the bow shock. They propagate toward the magnetopause, and the corresponding increase in $P_{\rm tot}$ is ~ 50-100% of the magnetosheath background value, as shown in Figure 10.

4. Parameter Search Based on the Ideal MHD

In this section, we use the ideal MHD formulation of the Riemann problem [*Lin and Lee*, 1994] to study the strength of the pressure pulse generated by the BS/RD interaction. The ideal MHD results are similar to those from hybrid simulations. A parameter search is performed to estimate the dependence of the pulse strength on various solar wind and bow shock conditions. According to the ideal MHD, rotational discontinuities RD1′ and RD2′, slow shocks SS1′ and SS2′, and contact discontinuity CD′ are generated by the BS/RD interaction, where RD1′ and RD2′ play the role of TDIS1′ and TDIS2′, respectively, in Case 1 as shown in Figure 3.

In the following search, the amplitude of the pressure pulse $\Delta P_{\rm tot}$ and the increase of the density $\Delta\rho$ are calculated at the leading edge of the pulse, i.e., at the rotational discontinuity RD1′. The simulation frame, which is described in section 2, is used in the calculation. In the normal incident frame of the bow shock, the amplitude of the pressure pulse is larger than that shown below.

Figure 11 shows the ratios $R_{\rm pre} \equiv \Delta P_{\rm tot}/P_{\rm tot2}$ and $R_\rho \equiv \Delta\rho/\rho_2$ as a function of M_A, θ_{Bn}, β_0, and $\Delta\Phi$. Here, the subscript "2" indicates the physical quantities in the background magnetosheath. For $\theta_{Bn} = 50°$, $\beta_0 = 0.5$, and $\Delta\Phi = 160°$, the dependence of $R_{\rm pre}$ (solid line) and R_ρ (dotted line) on M_A is plotted in the top left panel of Figure 11. The strength of the pressure pulse and the increase in plasma density which are caused by the BS/RD interaction are found to decrease as the Mach number M_A increases. For M_A in the range of ~ 3-8, the increase of the dynamic pressure $R_{\rm pre}$ is by ~ 30-120%. Note that in the hybrid simulation, the increase in the plasma density ρ is usually higher than in the MHD model because of the increase of density across the rotational discontinuity, which is caused by the pressure anisotropy.

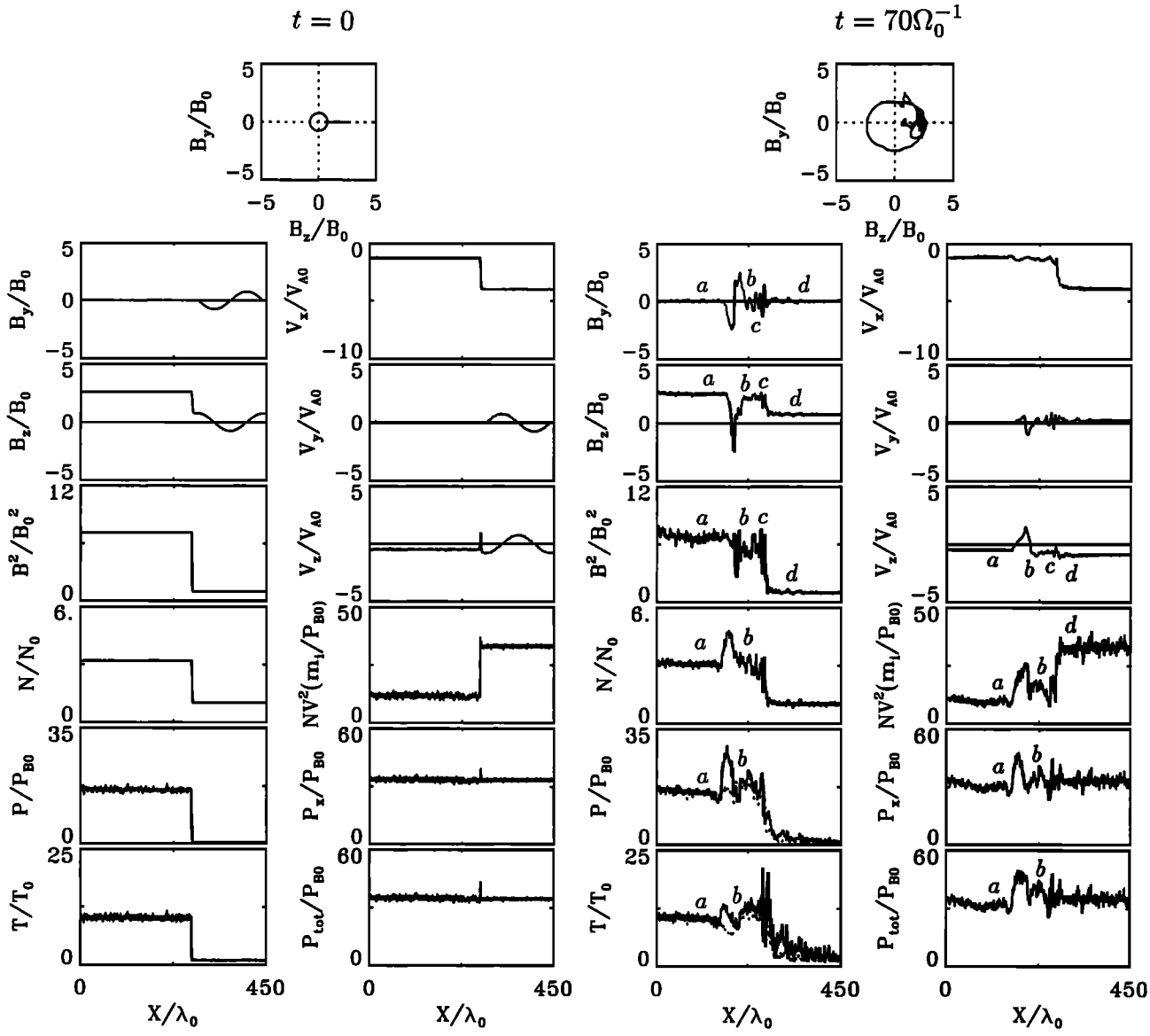

Figure 9. Hybrid simulation results of Case 3: field hodogram and spatial profiles of physical quantities at $t = 0$ and $t = 70\Omega_0^{-1}$.

In the top right panel of Figure 11, $R_{\rm pre}$ and R_ρ are plotted against β_0 for $M_A = 6$, $\theta_{Bn} = 50^o$, and $\Delta\Phi = 160^o$. As β_0 in the upstream solar wind increases, the pressure pulse becomes weaker. The strength of the pressure pulse as a function of the field rotation angle $\Delta\Phi$ is shown in the bottom left plot. The pulse amplitude increases with the field rotation angle. The maximum strength of the pressure pulse occurs at $\Delta\Phi = \pm 180^o$. At $\Delta\Phi = 0^o$, the initial rotational discontinuity RD does not exist, and thus no pressure pulse is generated. Therefore $R_{\rm pre} = R_\rho = 0$. In addition, the maximum strength of the pressure pulse is in the range of $\theta_{Bn} \simeq 50^o$-80^o, as seen in the bottom right plot of Figure 11.

5. Summary and Discussion

We have carried out 1-D MHD and hybrid simulations to study the interaction between the bow shock and an incoming rotational discontinuity, Alfven wave pulse, or Alfven wave train from the interplanetary space. In particular, the generation of dynamic pressure pulses by the BS/RD (BS/AW) interaction is investigated. A summary of the simulation results is given below.

1. For the interaction between the bow shock and a rotational discontinuity, the resistive MHD simulation shows that two TDISs, two slow shocks, and a contact discontinuity are generated in the magnetosheath downstream of the bow shock. The bow shock strength and location after the interaction are almost the same as those initially, and the rotation angle of the tangential magnetic field across one of the TDISs is much closer to the initial RD than across the other TDIS. A density enhancement and a magnetic field decrease are found throughout the resulting TDISs, slow shocks and the contact discontinuity in the magnetosheath, which propagate to the magnetopause. The sum of the magnetic and thermal pressure is nearly constant in the re-

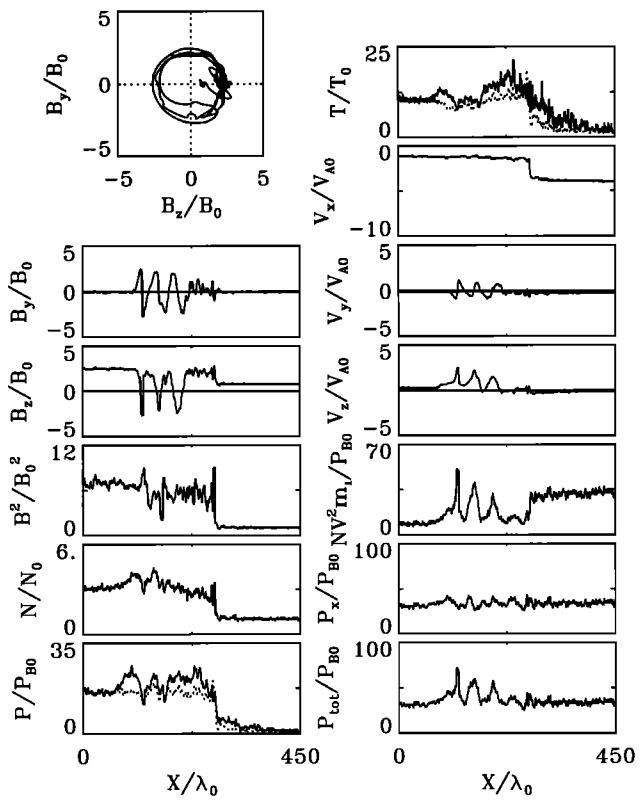

Figure 10. Hybrid simulation results of Case 4, in which an initial Alfven wave train with three 360° field rotations is incident on the bow shock. The hodogram and profiles are shown for $t = 110\Omega_0^{-1}$.

gion of density enhancement. There exists a strong dynamic pressure pulse in the ρV^2 profile in this region, which propagates with the discontinuities to the magnetopause. The total pressure $P_{\rm tot} = (P + B^2/2\mu_0 + \rho V^2)$ also increases correspondingly.

2. In the hybrid simulation of the BS/RD interaction, a rotational discontinuity with a field rotation angle nearly equal to the initial angle $\Delta\Phi$ appears in the region downstream from the bow shock. Two slow shocks are also found behind the rotational discontinuity. A strong pulse in the dynamic pressure NV^2, and thus in the total pressure $P_{\rm tot}$, is found at the downstream discontinuities. The increase of N at the pressure pulse is larger than that in the ideal MHD model because of the presence of a temperature anisotropy. In addition, the amplitude of the dynamic pressure pulse in the hybrid simulation is much larger than that in the resistive MHD model, because the rotational discontinuity is replaced by a TDIS in the resistive MHD and thus the acceleration of tangential flow is smaller. For $\theta_{Bn} \sim 50°$, $M_A \sim 6$, $\beta_0 \sim 0.5$, and $\Delta\Phi \sim 160°$, the amplitude of the $P_{\rm tot}$ pulse is $\sim 50\%$ (100% in the normal incident frame of the bow shock) of the background value in the magnetosheath. The pressure pulse propagates toward the magnetopause with a nearly constant amplitude. Note that the amplitude of the density pulse also remains constant.

The amplitude of the pressure pulse increases with the rotation angle $\Delta\Phi$ across the initial RD but decreases with the Alfven Mach number M_A and upstream plasma beta β_0 of the bow shock. In addition, the solution of the MHD Riemann problem associated with the BS/RD interaction shows that a maximum pressure pulse exists for the bow shock with a shock normal angle $\theta_{Bn} \sim 50°$-$80°$.

3. For the interaction between the bow shock and the Alfven wave pulse, the hybrid simulation shows that a large-amplitude Alfven wave with a field rotation angle $\sim \Delta\Phi$ is formed downstream of the bow shock. A density increase, magnetic field decrease, and a strong dynamic pressure pulse are present at this Alfven wave.

4. The interaction between the bow shock and an Alfven wave train is also simulated. After the interaction, an Alfven wave train is present downstream of the bow shock. A train of dynamic pressure pulses thus propagates in the magnetosheath to the magnetopause.

The substantial increase in the dynamic pressure NV^2 is mainly caused by the deflection of the flow tangential to the bow shock normal direction. The plasma flow parallel to the bow shock front may have a normal component at the magnetopause, especially at the locations away from the subsolar point. While the dynamic pressure pulse approaches and impinges on the magnetopause, it may compress the magnetopause globally and make an antisunward propagating ripple. The local-time dependence of the magnetospheric response to variations in the IMF orientation can be studied by 2-D simulations. The pressure pulse can contribute to the observed ionospheric traveling vortices [e.g., *Friis-Christensen et al.*, 1988; *Sibeck et al.*, 1989]. This may lead to the magnetic impulse events observed in the po-

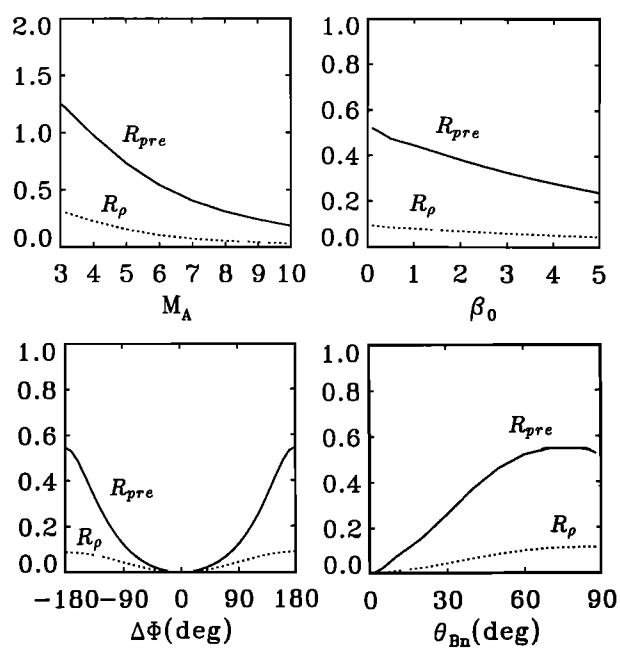

Figure 11. A parameter search for the strength of the pressure pulse based on the ideal MHD formulations of the Riemann problem associated with the BS/RD interaction. The ratios $R_{\rm pre} = \Delta P_{\rm tot}/P_{\rm tot2}$ (solid lines) and $R_\rho = \Delta\rho/\rho_2$ (dotted lines) are plotted against M_A, β_0, Φ, and θ_{Bn}.

lar ionosphere [*Lanzerotti et al.*, 1986]. Therefore our study suggests that the observed MIEs at high latitudes may be associated with variations in the IMF direction. A recent statistical study by *Konik et al.* [1994] indicated that over 50% of the observed MIE events are accompanied by variations in the IMF direction.

It must be emphasized that the variations in the IMF direction may also lead to other physical processes at the magnetopause. For example, bursty magnetic reconnections and FTEs at the dayside magnetopause may also be triggered by the pressure pulses formed by the changes of IMF direction.

The simulation study presented in this paper is based on 1-D models. Further investigations for the 2-D bow shock-magnetosheath-magnetopause system are necessary for our complete understanding of the generation of pressure pulses by IMF variations. In addition, reflected ions play an important role in the structure of the bow shock [e.g., *Scholer and Terasawa*, 1990]. If the upstream IMF suddenly changes direction, the reflected ions may move to a different position in the 2-D plane and then return to the bow shock at a position with a different local shock normal angle and Mach number. Therefore dynamic pressure pulses may be generated in the foreshock, and these upstream pressure pulses may then propagate to and interact with the bow shock and produce downstream pressure pulses. Satellite observations have shown that some of the observed pressure pulses upstream of the bow shock are associated with changing IMF directions, and the upstream dynamic pressure pulses correspond to compressions or rarefactions in the dayside magnetospheric magnetic field [*Fairfield et al.*, 1990]. A complete study could be carried out by including both quasi-parallel and quasi-perpendicular shocks.

Acknowledgments. YL would like to thank J. D. Perez for helpful discussions. This work was supported by the ONR grant NAVY-N00014-951-0839 to the Auburn University, NASA/SPTP grant NAG5-1504 to the University of Alaska, and a grant from National Science Council to the National Cheng Kung University.

The Editor thanks H. K. Biernat and D. G. Sibeck for their assistance in evaluating this paper.

References

Bering, E. A., III, J. R. Benbroof, G. J. Byrne, B. Liao, J. R. Theall, L. J. Lanzerotti, G. G. Maclennan, A. Wolfe, and G. L. Siscoe, Impulsive electric and magnetic field perturbations observed over South Pole: Flux transfer events?, *Geophys. Res. Lett., 15*, 1545, 1988.

Bering, E. A., III, L. J. Lanzerotti, J. R. Benbrook, and Z.-M. Lin, Solar wind properties observed during high-latitude impulsive perturbation events, *Geophys. Res. Lett., 17*, 579, 1990.

Burgess, D., Cyclic behavior at quasi-parallel collisionless shocks, *Geophys. Res. Lett., 16*, 345, 1989.

Burlaga, L. F., Directional discontinuities in the interplanetary magnetic field, *Sol. Phys., 7*, 57, 1969.

Denton, R. E., S. P. Gary, X. Li, B. J. Anderson, J. W. LaBelle, and M. Lessard, Low-frequency fluctuations in the magnetosheath near the magnetopause, *J. Geophys. Res., 100*, 5665, 1995.

Fairfield, D. H., W. Baumjohann, G. Paschmann, H. Luhr, and D. G. Sibeck, Upstream pressure variations associated with the bow shock and their effects on the magnetosphere, *J. Geophys. Res., 95*, 3773, 1990.

Farrugia, C. J., M. P., Freeman, S. W. H. Cowley, D. J. Southwood, M. Lockwood, and A. Etemadi, Pressure-driven magnetopause motions and attendant response on the ground, *Planet. Space Sci., 37*, 589, 1989.

Friis-Christensen, M., A. McHenry, C. R. Clauer, and S. Vennerstrom, Ionospheric traveling convection vortices observed near the polar cleft: A triggered response to sudden change in the solar wind, *Geophys. Res. Lett., 15*, 253, 1988.

Glassmeier, K.-H., and C. Heppner, Traveling magnetospheric convection twin vortices: Another case study, global characteristics, and a model, *J. Geophys. Res., 97*, 3977, 1992.

Glassmeier K.-H., M. Hoenisch, and J. Untiedt, Ground-based and satellite observations of traveling magnetospheric convection twin vortices, *J. Geophys. Res., 94*, 2520, 1989.

Goodrich, C. C., and P. J. Cargill, An investigation of the structure of rotational discontinuities, *Geophys. Res. Lett., 18*, 65, 1991.

Hassam, A. B., Transmission of Alfven waves through the Earth's bow shock: Theory and observation, *J. Geophys. Res., 83*, 643, 1978.

Hubert, D., Nature and origin of wave modes in the dayside magnetosheath, *Adv. Space Res.*, in press, 1994.

Jeffrey, A., and T. Taniuti, *Non-Linear Wave Propagation*, Academic, San Diego, Calif., 1964.

Kaufmann, R. L., and A. Konradi, Explorer 12 magnetopause observations: Large-scale nonuniform motion, *J. Geophys. Res., 74*, 3609, 1969.

Konik, R. M., L. J. Lanzerotti, A. Wolfe, C. G. Maclennan, and D. Venkatesan, Cusp latitude magnetic impulse events, 2, Interplanetary magnetic field and solar wind conditions, *J. Geophys. Res., 99*, 14,931, 1994.

Landau, L. D., and E. M. Lifshitz, *Fluid Mechanics*, Pergamon, Tarrytown, N. Y., 1959.

Landau, L. D., and E. M. Lifshitz, *Electrodynamics of Continuous Media*, Pergamon, Tarrytown, N. Y., 1960.

Lanzerotti, L. J., Comment on "Solar wind dynamic pressure variations and transient magnetospheric signatures," *Geophys. Res. Lett., 16*, 1197, 1989.

Lanzerotti, L. J., L. C. Lee, C. G. Maclennan, A. Wolfe, and L. V. Medford, Possible evidence of flux transfer events in the polar ionosphere, *Geophys. Res. Lett., 13*, 1089, 1986.

Lanzerotti, L. J., R. D. Hunsucker, D. Rice, L. C. Lee, A. Wolfe, C. G. Maclennan, and L. V. Medford, Ionospheric and ground-based response to field-aligned currents near the magnetospheric cusp regions, *J. Geophys. Res., 92*, 7739, 1987.

Lanzerotti, L. J., R. M. Konik, A. Wolfe, D. Venkatesan, and C. G. Maclennan, Cusp-latitude magnetic impulse events, 1., Occurrence statistics, *J. Geophys. Res., 96*, 14,009, 1991.

Lee, L. C., Magnetic flux transfer at the Earth's magnetopause, in *Proceedings of Chapman Conference on Solar Wind-Magnetosphere Coupling*, edited by Y. Kamide and J. Slavin, p. 297, Terra Sci., Tokyo, 1986.

Lee, L. C., L. Huang, and J. K. Chao, On the stability of rotational discontinuities and intermediate shocks, *J. Geophys. Res., 94*, 8813, 1989.

Lin, Y., and L. C. Lee, Structure of the dayside reconnection layer in resistive MHD and hybrid model, *J. Geophys. Res., 98*, 3919, 1993.

Lin, Y., and L. C. Lee, Structure of reconnection layers in the magnetosphere, *Space Sci. Rev., 65*, 59, 1994.

Lin, Y., L. C. Lee, and C. F. Kennel, The role of intermediate shocks in magnetic reconnection, *Geophys. Res. Lett., 19*, 229, 1992.

Lysak, R. L., Y. Song, and D.-H. Lee, Generation of ULF waves by fluctuations in the magnetopause position, in *Solar Wind Sources of Magnetospheric Ultra-Low-Frequency Waves, Geophys. Monogr. Ser.*, vol. 81, edited by M. J. Engebretson, K. Takahashi, and M. Scholer, p. 273, AGU, Washington, D. C., 1994.

Lyu, L. H., and J. R. Kan, Ion leakage, ion reflection, ion heating and shock-front reformation in a simulated supercritical quasi-parallel collisionless shock, *Geophys. Res. Lett., 17*, 1041, 1990.

Mandt, M. E., and L. C. Lee, Generation of Pc 1 waves by the ion temperature anisotropy associated with fast shocks caused by sudden impulses, *J. Geophys. Res., 96*, 17,897, 1991.

Richter, P., and M. Scholer, On the stability of rotational discontinuities, *Geophys. Res. Lett., 16*, 1257, 1989.

Russell, C. T., and R. C. Elphic, Initial ISEE magnetometer results: Magnetopause observations, *Space Sci. Rev., 22*, 691, 1978.

Saunders, M. A., C. T. Russell, and N. Sckopke, Flux transfer events: Scale size and interior structure, *Geophys. Res. Lett., 11*, 131, 1984.

Scholer, M., and T. Terasawa, Ion reflection and dissipation at quasi-parallel collisionless shocks, *Geophys. Res. Lett., 17*, 119, 1990.

Sibeck, D. G., Quantifying the magnetospheric response to solar wind dynamic pressure variations, *Physics of Space Plasmas (1990)*, edited by T. Chang et al., p. 393, Sci. Publ., Cambridge, Maryland, 1991.

Sibeck, D. G., W. Baumjohann, and R. E. Lopez, Solar wind dynamic pressure variations and transient magnetospheric signatures, *Geophys. Res. Lett., 16*, 13, 1989.

Song, P., C. T. Russell, and M. F. Thomsen, Slow mode transition in the frontside magnetosheath, *J. Geophys. Res., 97*, 8295, 1992.

Southwood, D. J., The hydromagnetic stability of the magnetospheric boundary, *Planet. Space Sci., 16*, 587, 1968.

Southwood, D. J., Theoretical aspects of ionosphere-magnetosphere solar wind coupling, *Adv. Space Res., 5(4)*, 7, 1985.

Southwood, D. J., The ionospheric signature of flux transfer events, *J. Geophys. Res., 92*, 3207, 1987.

Southwood, D. J., and M. G. Kivelson, The magnetohydrodynamic response of the magnetospheric cavity to changes in solar wind pressure, *J. Geophys. Res., 95*, 2301, 1990.

Swift, D. W., and L. C. Lee, Rotational discontinuities and the structure of the magnetopause, *J. Geophys. Res., 88*, 111, 1983.

Wu, B. H., M. E. Mandt, L. C. Lee, and J. K. Chao, Magnetospheric response to solar wind dynamic pressure variations: Interaction of interplanetary tangential discontinuities with the bow shock, *J. Geophys. Res., 98*, 21,297, 1993.

Wu, C. C., and C. F. Kennel, Structure and evolution of time-dependent intermediate shocks, *Phys. Rev. Lett., 68*, 56, 1992.

Yan, M., and L. C. Lee, Generation of slow-mode waves in front of the dayside magnetopause, *Geophys. Res. Lett., 21*, 629, 1994.

Yan, M., and L. C. Lee, Interaction of interplanetary shocks and rotational discontinuities with the Earth's bow shock, *J. Geophys. Res.*, in press, 1995.

L. C. Lee, College of Science, National Cheng Kung University, Tainan, Taiwan.

Y. Lin, Physics Department, 206 Allison Lab, Auburn University, Auburn, AL 36849-5311.

M. Yan, Geopyhsical Institute and Department of Physics, University of Alaska, Fairbanks, AK 99775-7320.

(Received May 22, 1995; revised September 5, 1995; accepted September 27, 1995.)